Inorganic Chemistry

Forum Article

pubs.acs.org/IC

Strategies toward High-Temperature Lanthanide-Based Single-Molecule Magnets

Liviu Ungur*[,†,‡] and Liviu F. Chibotaru*[,†]

[†]Theory of Nanomaterials Group, Chemistry Department, Katholieke Universiteit Leuven, Celestijnenlaan 200F, 3001 Leuven, Belgium

[‡]Chemistry Department, Lund University, Getingevagen 60, 22201 Lund, Sweden

ABSTRACT: Lanthanide-based single-molecule magnets are leading materials for achieving magnetization blocking at the level of one molecule. In this paper, we examine the physical requirements for efficient magnetization blocking in single-ion complexes and identify the design principles for achieving very high magnetization blocking barriers in lanthanide-based compounds. The key condition is the preponderant covalent binding of the Ln ion to one of the ligand atoms, tremendously enhancing the axial crystal field. We also make an overview of practical schemes for the implementation of this principle. These are (1) the effective lowering of the coordination number via displacement of the Ln ion to one of the atoms in the coordination polyhedron, (2) the design of two-coordinated complexes, and (3) the stabilization of diatomic compounds in cages and on surfaces. The last proposal is appealing in connection to spintronics applications, especially via the exploration of robust and highly anisotropic [LnX] units displaying multilevel blocking barriers of thousands of Kelvin and prospects for room-temperature magnetization blocking.

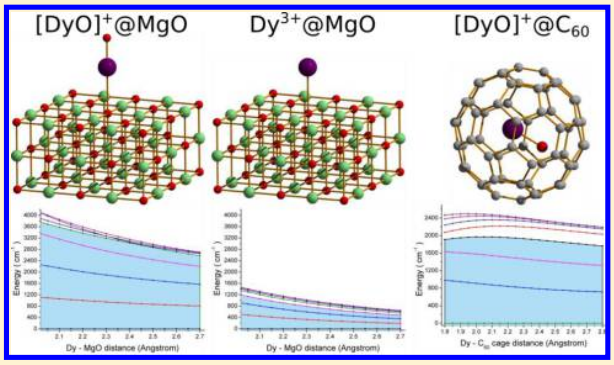

INTRODUCTION

Single-molecule magnets (SMMs) are regarded as potential candidates for various applications in molecular electronics,[1−18] first of all as elements for high-density data storage devices.[19−22] The main requirement for the latter is the ability to block magnetization at elevated temperature. This is quantified by the so-called blocking temperature (T_B), which in the case of SMMs means the highest temperature at which the magnetization is preserved during a given period of time, e.g., 100 s.[19] For instance, in Mn_{12}ac subject to a minimal bias magnetic field, sufficient to suppress the quantum tunneling of magnetization (QTM) in the ground state, T_B = 2.5 K.[19] This can be measured from recovery magnetization functions $M(t)$.[20,23] Another way to detect magnetization blocking is via the observation of magnetic hysteresis loops.[24,25] These show up in SMMs starting with some value of the field-sweep rate, specific for a given temperature. Therefore, T_B is defined as a temperature at which the magnetic hysteresis disappears at some reference field-sweep rate.[26,27]

The first discovered SMMs, Mn_{12}ac and Fe_8,[28] were polynuclear complexes, in which magnetization blocking was achieved through zero-field splitting (ZFS) of the ground-state exchange term S = 10. The key requirement for the appearance of magnetization blocking in such complexes is the dominant negative axial component of ZFS, while the large S ensures suppression of the QTM in the ground and several excited exchange doublet states.[19] The lowest doublet state through which intensive tunneling relaxation of magnetization occurs at a given temperature defines the height of the blocking barrier, U_{eff}, in the activation mechanism of relaxation.[19,29] This mechanism becomes dominant at relatively high temperatures, when its rate of activation relaxation, $\tau^{-1} = \tau_0^{-1} \exp\left(-\frac{U_{eff}}{kT}\right)$, exceeds the QTM relaxation rate, where τ is the relaxation time for magnetization.[20,30,31] The important feature of these SMMs is the multilevel character of the blocking barriers because of which the relaxation path includes a sequential spin-phonon transition between several exchange levels from the bottom to the top of the barriers.[29,32] This allows one to significantly reduce the prefactor τ_0^{-1} in the expression for the activation relaxation rate because it depends on the energy intervals ΔE between neighboring exchange levels in the relaxation path as ΔE^3.[33]

A decade later, the magnetization blocking effect was demonstrated for mononuclear lanthanide bis-(phthalocyaninato) molecules,[34] in which the magnetization blocking barrier corresponded to the first excited crystal-field (CF) doublet state of the complexes.[35] This discovery ignited broad interest in the study of slow magnetic relaxation in mononuclear lanthanide-based SMMs.[36−43] Besides lantha-

Special Issue: New Trends and Applications for Lanthanides

Received: June 7, 2016
Published: August 10, 2016

DOI: 10.1021/acs.inorgchem.6b01353
Inorg. Chem. 2016, 55, 10043−10056

nides, magnetization blocking in mononuclear transition-metal and actinide complexes started to be intensively investigated.[42,44−49] However, compared to lanthanide mononuclear complexes, they seem to demonstrate less efficient magnetization blocking.[50,51] On the contrary, mononuclear lanthanides proved to be as efficient SMMs as polynuclear complexes, with blocking barriers on the order of 1000 K,[52,53] magnetic hysteresis loops with remanence on the order of 1−2 Tesla[54−57] persistance until T_B = 20−30 K,[56,57] and a relaxation time of 1500 s at 10 K[56] in diluted compounds.

The better SMM performance of lanthanides compared to other mononuclear metal complexes is generally explained by a weaker metal−ligand covalence combined with a very strong spin−orbit coupling, resulting in much larger unquenched angular and magnetic moments.[58] Given the leading role of lanthanide complexes among promising materials for magnetization blocking, it is of primary interest to outline the strategy for further enhancement of their SMM properties. In this Forum Article, we attempt to answer these questions by analyzing the known facts about lanthanide SMMs and on the basis of additional theoretical studies. In the first part of the article, we overview the physical requirements for designing efficient SMMs on the basis of lanthanide complexes. In the second part, we propose practical solutions for the implementation of suitable schemes into real complexes/magnetic structures. Approaches preserving high blocking characteristics for trapped and deposited complexes are emphasized in view of their potential applications in molecular spintronics.

FACTORS INFLUENCING MAGNETIZATION BLOCKING

The purposeful design of efficient SMMs requires a detailed knowledge of the factors influencing the blocking of magnetization in complexes. Here we review these factors with emphasis on lanthanides.

What is an Efficient SMM? It is by definition a complex able to retain its magnetization for a long period of time (compared to the measuring time) and at relatively elevated temperature.[19] Figure 1 shows the generic structure of low-lying multiplet levels in SMMs. It involves separated doublets of time-reversed states, characterized by equal magnetizations of opposite sign (|M| and −|M|) along the main magnetic axis of the respective doublet. Each doublet is exactly degenerate in complexes with an odd number of electrons (Kramers doublets, KDs) or quasidegenerate in complexes with an odd number of electrons.[59] Some of the non-KDs can be exactly degenerate as well in high-symmetry complexes (Ising doublets),[60] albeit this situation is not often encountered for SMMs, which are either embedded in a crystal or deposited on a surface. The multiplets correspond to ZFS exchange states in the case of polynuclear complexes[20] or to CF multiplets in mononuclear complexes.[34] Although in the early SMM complexes M monotonically decreased with the number of excited doublet states (as shown in Figure 1),[19] this is actually not an indispensable feature of SMMs.[61]

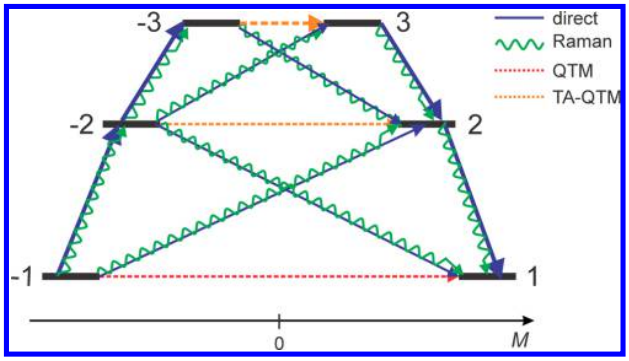

Figure 1. Scheme of spin−orbit doublet states (±n) corresponding to ZFS components of the ground-state S term or to CF components of the ground-state atomic J multiplet. The two states of a doublet have opposite values of magnetization, |M| and −|M|, respectively. The arrows show the mechanisms of relaxation of magnetization (see the text). An ideal SMM corresponds to the suppression of all relaxation channels except for the ones shown by bold arrows.

The necessary condition for a complex to display blocking of magnetization in a given temperature domain is the sufficiently low rate of QTM relaxation flipping of the magnetization $M \leftrightarrow -M$ in the ground doublet state. More precisely, the QTM relaxation rate should be so low as to allow its suppression at relatively weak direct-current (dc) magnetic fields, on the order of the internal field in the crystal, sufficient to bring the two ground doublet state levels out of resonance.[20,62] Increasing the separation between these levels will activate the direct relaxation process, which is the case when an external dc magnetic field, much larger than the internal one, is applied.[63,64] Besides this, with an increase of the temperature, two other relaxation mechanisms come into play: first the second-order (resonant) Raman and then the Orbach process.[59] Both are two-phonon relaxation mechanisms involving the first excited doublet state via the two-step transitions −1 → −2 → 1 and −1 → 2 → 1 (Figure 1). The difference is that in the Raman relaxation the absorption of one phonon (transition −1 → ±2) and the emission of the other one (transition ±2 → 1) are virtual processes, while in the Orbach relaxation, they are real (corresponding to two direct spin-phonon transitions). These are the main relaxation processes in systems lacking strong axiality (discussed below) such as Ln^{III} ions embedded in various crystals.[65−67] However, in performant lanthanide SMMs, they are strongly suppressed,[58] the same for the temperature-assisted quantum tunneling of magnetization (TA-QTM)[68] in the first excited doublet state. In this case, relaxation proceeds from the first excited doublet state, n = 2, via the second excited doublet state, n = 3 (Figure 1), involving the same processes as those described above. If these indirect relaxation mechanisms (Raman and Orbach) connecting the states −2 and +2 are efficiently suppressed, relaxation proceeds via the third excited doublet state, etc. Then the relaxation path will involve only direct spin-phonon transitions between neighboring multiplet states (bold arrows in Figure 1). Each such transition requires the absorption of one phonon when climbing the stair of states; i.e., it is of the activation type.[59] Therefore, the relaxation rate is described by an Arrhenius low mentioned above,[19] in which the barrier height U_{eff} corresponds to the highest involved doublet state (n = 3 in Figure 1).

An efficient SMM is characterized by a high multistep activation barrier, i.e., involving as many doublet states as can be offered by the multiplet structure of the complex. To achieve this situation, the unwanted relaxation processes (thin arrowed lines in Figure 1) should be efficiently suppressed. Each process represents a spin−orbit transition between the connected multiplet states, which is described by the Fermi golden rule.[19,59] The corresponding expression involves a transition

DOI: 10.1021/acs.inorgchem.6b01353
Inorg. Chem. 2016, 55, 10043−10056

matrix element of an electronic operator and a temperature-dependent phonon factor. The design of a complex is directed toward engineering the structure of its low-lying multiplet states, which affects first of all the electronic transition matrix elements in various relaxation processes. Then knowledge of their dependence on the details of multiplet structure becomes of practical importance. In the following, we discuss the factors defining the most efficient multiplet structure of lanthanide complexes from the point of view of their SMM performance.

Optimal Structure of CF Multiplets. In lanthanide complexes, the low-lying spin−orbit multiplets basically arise from CF splitting of the ground-state atomic J multiplet of the corresponding Ln^{III} ion.[69] Accordingly, the corresponding wave functions can be represented as linear combinations of the eigenfunctions $|Jm\rangle$ of the atomic J multiplet of the Ln^{III} ion:

$$|n\rangle = \sum_{m=-J}^{J} c_{nm}|Jm\rangle$$

$$|-n\rangle = \theta|n\rangle = \sum_{m'=-J}^{J} (-1)^{J+m'} c_{n-m'}{}^{*}|Jm'\rangle \quad (1)$$

where n is the number of CF doublets, θ is the time-reversal operator, and m is the projection of the total angular momentum J on a given axis z. The coefficients c_{nm}, defining the doublet eigenfunctions in eq 1, are obtained from diagonalization of the CF operator:

$$\hat{H}_{CF} = \sum_{p} \sum_{k=-p}^{p} B_{pk} O_p^k(\hat{J}) \quad (2)$$

where $O_p{}^k$ is the (complex) Stevens operator[59] representing a polynomial of rank p of the projections of the total angular momentum J_α, where $\alpha = x, y, z$. It is believed that the CF operator (2) describes the splitting of atomic orbitals,[70] in which case it contains only even-rank operators, which in the case of the 4f shell correspond to $p = 2, 4, 6$.[59,71]

The spin-phonon transitions between doublet states are caused by dynamical deformations of the environment.[19] The operator causing this transition is similar to eq 2 in which the CF parameters are now functions of the displacements q_i of the ligand atoms, $B_{pk}(\{q_i\})$. The electronic part of this operator contains terms of the form $b_{pk}O_p{}^k$, where the constants b_{pk} are first derivatives of $B_{pk}(\{q_i\})$ after q_i in the case of direct spin-phonon transitions and second derivatives after q_i and q_j in the case of Raman transitions. Then the electronic transition matrix elements connecting the doublet states with reversed magnetization (Figure 1) are of the following form:

$$\langle -n|b_{pk}O_p^k(\hat{\mathbf{J}})|n'\rangle = \frac{b_{pk}}{k_p}\langle J\|O_p\|J\rangle \sum_{m=-J}^{J}\sum_{m'=-J}^{J} (-1)^{J+m} c_{n-m}c_{n'm'}C_{pkJm'}^{Jm} \quad (3)$$

where the reduced matrix element $\langle J\|O_p\|J\rangle$ and the constant k_p are defined in ref 73 and $C_{pkJm'}^{Jm}$ is the Clebsh−Gordan coefficient.[74] The latter is only different from zero when $k = m - m'$. This means that all terms on the right-hand-side of eq 3 will be zero if all $|Jm\rangle$ entering $|-n\rangle$ and all $|Jm'\rangle$ entering $|n'\rangle$, eq 1, have angular momentum projections obeying the relationship $m - m' \neq k$. Given that the maximal value of k in eq 2 is ±6 (but see the comment in ref 71) while the maximal value of m or m' (for Ho^{3+}) is ±8, it is well possible that under the optimal design of the doublet wave functions the phonon-induced transitions between many CF multiplet components will be completely blocked. The *optimal structure* of CF multiplets implies, therefore, a *large difference* between the projections m of the $|Jm\rangle$ eigenfunctions constituting the doublet states $|-n\rangle$ (left-hand side of Figure 1) from the projections m' of the $|Jm'\rangle$ eigenfunctions constituting the doublet states $|n'\rangle$ (right-hand side of Figure 1). This situation is achieved, e.g., for a very high axial symmetry of CF at the location of the Ln ion, in which case most doublets are $|\pm n\rangle \approx |J \pm |m|\rangle$.

Actually, not all terms $b_{pk}O_p{}^k$ in the spin-phonon transition operator are equally important. In the case of pure spin systems, such as Mn_{12}ac, only the second-rank terms are relevant, with the major contribution being the rotation of the main anisotropy axis of the ground spin induced by vibrations.[29,32,33] The corresponding electronic transition operators are of the form of an anticommutator $\sim\{S_\alpha, S_z\}$, where z is the direction of the main anisotropy axis and $\alpha = x, y$.[19] In lanthanides, the "rotational" contributions to the spin-phonon interaction are of the form $\sim\{J_\alpha, J_z\}$[75,76] and are assumed to be dominant as well.

Axiality of CF Doublets. The phonon factor defining the transition rate of the direct (and Orbach) process scales as a third power of the energy separation between the corresponding levels.[59] Therefore, this process will not contribute to the relaxation between the two components $|-n\rangle$ and $|n\rangle$ of a given doublet, if this is not subject to a strong bias magnetic field.[76−78] In this case, the relaxation between the two components of a doublet can proceed via the QTM for the ground state and via the TA-QTM for the excited doublet state. Whatever the specific mechanism of tunneling relaxation, via interaction with a phonon bath,[29,32,79] via hyperfine interaction with a nuclear spins bath,[80−82] or via interactions with fluctuations of dipolar magnetic fields (magnon bath),[83−85] its rate always scales as a square of the tunneling gap Δ^2_{tun} of the corresponding doublet.[19,86] This gap can be intrinsic (Δ_{int}) in complexes with an even number of electrons (non-Kramers complexes) or a Zeeman splitting induced by a magnetic field in complexes with an odd number of electrons (Kramers complexes). In the latter case, it has the form $2\Delta_{tun} = \mu_B[g_x{}^2H_x{}^2 + g_y{}^2 H_y{}^2]^{1/2}$, where g_x and g_y are transversal g factors of the doublet, corresponding to perpendicular directions to its main magnetic axis, and H_x and H_y are respective components of the magnetic field.

The quality characterizing the smallness of the tunneling gap is called the *axiality* of the doublet.[77] Then the necessary condition for SMM behavior is the requirement of high axiality of the ground doublet state: its sufficiently small Δ_{int} for non-Kramers complexes and its sufficiently small g_x and g_y for the Kramers ones. These are defined by the following matrix elements:

$$\Delta_{int} = \langle -n|\hat{H}_{CF}|n\rangle$$

$$g_{x,y} = 2\langle -n|\hat{\mu}_{x,y}|n\rangle/\mu_B \quad (4)$$

where the magnetic moment acquires a simple form, $\mu = -g_J\mu_B\mathbf{J}$, in the phenomenological CF description, which neglects metal−ligand covalency.[59] These matrix elements are of structure similar to that of eq 3 ($J_\alpha \sim O_1^\alpha$[74]); therefore, all arguments given there are equally applicable to the present case. In particular, the quantities in eq 4 will be suppressed

DOI: 10.1021/acs.inorgchem.6b01353
Inorg. Chem. 2016, 55, 10043−10056

under the conditions for the optimal structure of CF multiplets, requiring a large difference between all $|Jm\rangle$ entering $|n\rangle$ and all $|Jm'\rangle$ entering $|-n\rangle$ (eq 1). As was already mentioned, this situation is achieved for a strongly axial CF. Quantitatively, this means that the axial CF parameters B_{20}, B_{40}, and B_{60} in eq 2 considerably exceed the nonaxial CF parameters B_{pk} with $k \neq 0$. In this case, the doublet wave functions acquire a strongly axial character, $|\pm n\rangle \approx |J \pm |m|\rangle$.

Such Ising character of the doublet wave functions allows one to reduce the transition matrix elements of "rotational" contributions to the spin-phonon interaction, $\sim\{J_\alpha, J_z\}$, to the matrix elements of the corresponding J_α or μ_α (see above), where $\alpha = x, y$ is the transversal direction to the main magnetic axis (z) of the doublet. Then the electronic matrix element defining the spin-phonon transition is proportional to the transition magnetic moment matrix element between the corresponding states, the average of which can be written as follows:[77,87]

$$\bar{\mu}_{-n,n'} = \frac{1}{3}(|\mu_x| + |\mu_y| + |\mu_z|)$$
$$|\mu_\alpha| \equiv |\langle n|\hat{\mu}_\alpha|n'\rangle| \quad (5)$$

where the Cartesian components $\alpha = x, y, z$ correspond to a general coordinate system. The spin-phonon transition rate between $|-n\rangle$ and $|n'\rangle$ scales as a square of $\bar{\mu}_{-n,n'}$.[88] This allows one to use the latter for the assessment of the relative importance of relaxation paths between various states and, finally, to outline the relaxation barrier.[58,87]

For a perfectly axial CF, in which all B_{pk} with $k \neq 0$ are zero, the doublet wave functions are precisely $|J \pm |m|\rangle$ in the phenomenological CF approximation. Note that the total angular momentum projection m remains a good quantum number also when covalent effects are taken into account (the multiplet wave functions are not of the pure 4f type). Examples of this type are diatomic complexes such as $[DyO]^+$.[77] In such systems, the rotation/libration nuclear motions are the only cause for the spin-phonon transition. From eq 5, we see that only transitions between states differing by $\Delta m = \pm 1$ are allowed. Figure 2 shows the resulting blocking barrier, which thus involves all CF multiplets and has a height equal to that of the total CF splitting of the atomic J multiplet. We may conclude, therefore, that the highest possible performance of lanthanide-based SMMs is achieved in the limit of a perfectly axial CF in these complexes.

Geometry, Symmetry, and Coordination Numbers. Lanthanide complexes are characterized by various geometries of the environment and coordination numbers of nearest-neighbor atoms.[69] To assess a general dependence of the CF multiplet structure on the geometry and symmetry of the environment, we show in Figure 3 the results for several complexes with n equivalent monatomic ligands (n = 1−12). The obtained CF spectra clearly show that low coordination numbers, in combination with uniaxial symmetry (the complex for n = 2 is a linear F−Dy−F), lead to the largest CF splitting. The closer the distribution of the ligands to spherical symmetry, the smaller the CF splitting. Moreover, the environment of cubic (cube, octahedron, and tetrahedron) and icosahedral symmetry preserves the isotropy of the three Cartesian axes; i.e., such complexes cannot be SMM in principle. Axial complexes such as the two bipyramidal ones shown in Figure 3, as well as monopyramidal, prismatic, etc., will possess anisotropic doublet states. However, their axiality

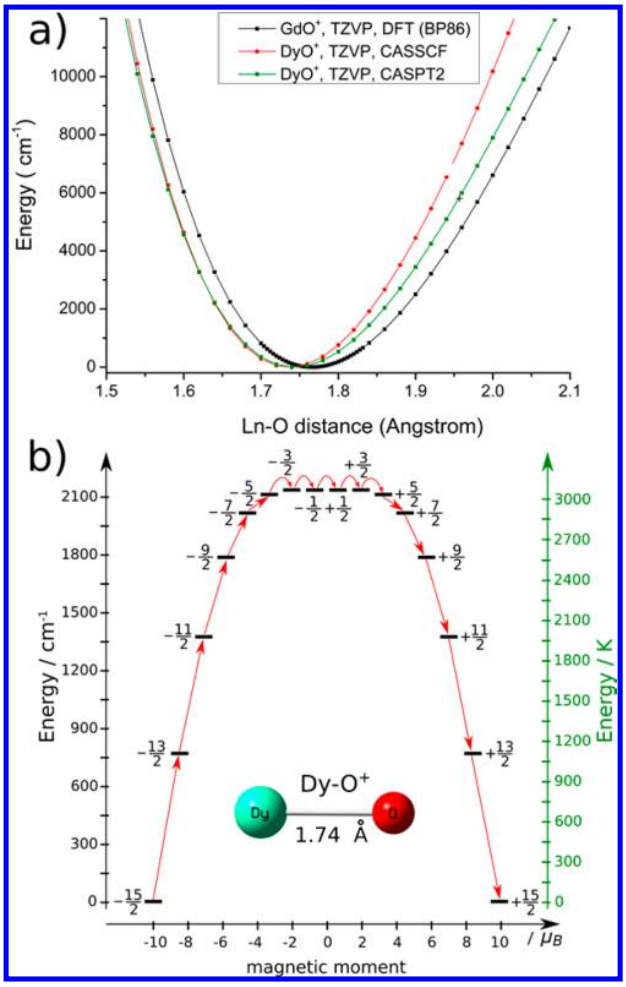

Figure 2. Ab initio optimized geometry (up) and calculated low-lying spectrum of doublet states (down) for the $[DyO]^+$ complex. The numbers at each level (horizontal bold lines) are m values of the corresponding multiplet state. Arrows show the allowed spin-phonon transitions. Adapted with permission from ref 77. Copyright 2011 Royal Society of Chemistry.

and the extent of CF splitting depend on the ratio between the axial CF contribution (coming from the two atoms in the axial positions) and the equatorial CF contribution (coming from n − 2 atoms in the equatorial plane), which should differ in strength as much as possible. The strongest axiality of the doublets and the maximal extent of CF splitting are achieved in the limit when one of these contributions vanishes, such as for the case where n = 1 and 2 in Figure 3.

One should note that complexes belonging to the axial symmetry group, such as trigonal and pentagonal bipyramids of D_{3h} and D_{5h} symmetry, respectively (Figure 3), can possess doublets of perfect axiality.[77] This is particularly the case of the first synthesized single-ion SMM, the double-decker phthalocyanine complex $[Tb(Pc)_2]^-$.[34] However, if the order of the main rotational axes in such complexes is lower than 8, the doublet wave functions are not eigenfunctions of the total angular momentum projection on the symmetry axis of the complex, $|Jm\rangle$, but rather their linear combinations.[69] This means that, according to eq 3, there will be unquenched spin-phonon transitions between the states $|-n\rangle$ and $|n'\rangle$ even if both or some of them belong to perfectly axial doublets.

DOI: 10.1021/acs.inorgchem.6b01353
Inorg. Chem. 2016, 55, 10043−10056

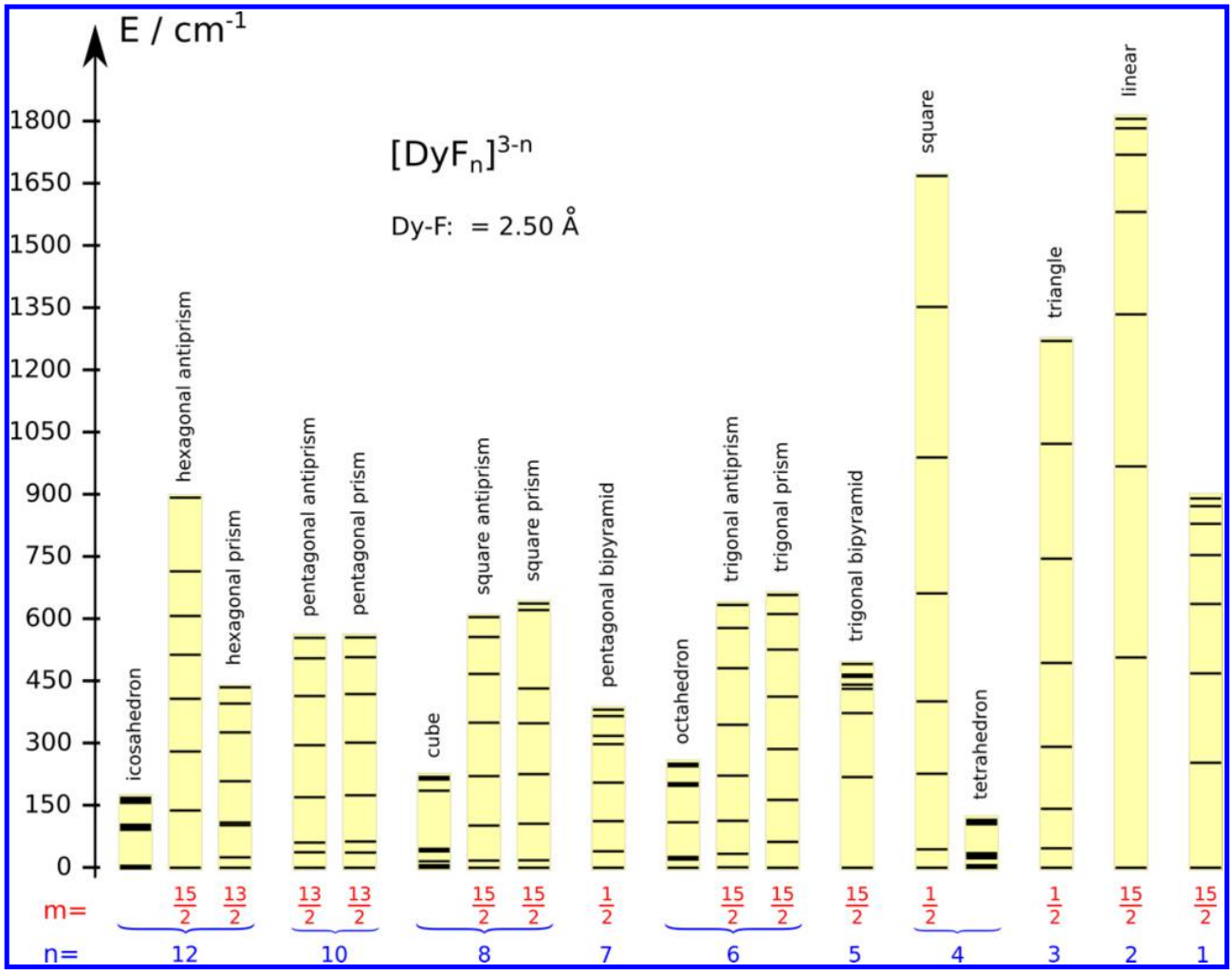

Figure 3. Structure of CF doublets of the ground-state $J = {}^{15}/_{2}$ manifold of hypothetical $[DyF_n]^{3-n}$ complexes of three-valent dysprosium, calculated ab initio for various coordination geometries at an arbitrary fixed Dy−F distance (2.50 Å). The coordination numbers are given at the bottom. m indicates the projection of the total angular momenta J in the ground KD state. For the icosahedron, cube, and tetrahedron, the ground state is Γ_8 (4-fold degenerate) and is magnetically isotropic (i.e., with no preferred orientation of magnetization). The ground doublet state of the octahedral structure is also isotropic.

We may conclude that the best geometries for a performant SMM are either axial, with one or two atoms axially bound to the Ln ion, or equatorial/sandwiched with the order or rotational axis $n > 7$.

High J and Main Magnetic Axes of CF Doublets. The geometry of the nearest ligand environment of Ln ions usually does not have any symmetry, especially in polynuclear complexes. Nevertheless, the axiality of such mononuclear complexes and fragments is high in the majority of cases, especially for the late Ln ions, which causes their SMM behavior.[42] The ultimate reason for that is the relatively large value of J.[58] Indeed, if we retain only the axial components of the CF, that is, B_{20}, B_{40}, and B_{60}, defined with respect to the main magnetic axis of the ground doublet state, the latter will become of the pure Ising type, $|Jm\rangle$, with m either coinciding with or being close to $\pm J$. Then the nonzero value of Δ_{int} or $g_{x,y}$ is achieved through the consecutive admixture of excited $|Jm'\rangle$ via the nonaxial CF components $\sim B_{pk}$, where $k \neq 0$, which connect the zeroth-order ground doublet states $|J_-|m|\rangle$ and $|J|m|\rangle$. The number of such admixture steps (the order of the perturbation theory) depends on the value of $|m|$. When the latter is large, the required order of the perturbation theory is high and the obtained Δ_{int} or $g_{x,y}$ is sufficiently small, thus providing high axiality of the corresponding doublet even for the low-symmetric environment of the Ln ion. An example is the $[Tb(Pc)_2]^-$ complex mentioned above, in which non-negligible deviations from an ideal D_{4d} symmetry result in the opening of a very small intrinsic gap, $\sim 10^{-6}$ cm^{-1}, in the ground doublet state ($|m| = J = 6$). This situation is common also for other late Ln ions such as Dy^{3+} ($J = {}^{15}/_{2}$), Ho^{3+} ($J = 8$), and Er^{3+} ($J = {}^{15}/_{2}$). Following this argument, the relative smallness of the total angular momentum in transition-metal and actinide complexes explains why they can only be SMM in high-symmetric (trigonal) geometry[42,44−51] but not in a low-symmetry structure.

The ab initio calculations have shown that, in low-symmetry complexes and fragments, the late Ln ions can display strong axiality not only for the ground state but also for several excited doublet states.[77] However, the main magnetic axes of these doublets display relative rotations that may amount in some

DOI: 10.1021/acs.inorgchem.6b01353
Inorg. Chem. 2016, 55, 10043−10056

cases to tens of degrees.[77] This relative rotation of the main magnetic axes is a major mechanism of spin-phonon transitions between strongly axial doublet states. Indeed, even if the latter are almost of the Ising type, $|-n\rangle \approx |Jm\rangle$ and $|n'\rangle \approx |Jm'\rangle$, with $m - m'$ large enough to suppress the spin-phonon transition according to the arguments given after eq 3, this paradigm will not apply if $|Jm\rangle$ and $|Jm'\rangle$ are defined with respect to different quantization axes. Indeed, in the latter case, the state $|Jm'\rangle$ can be decomposed into a linear combination of eigenstates $|Jm''\rangle$ defined with respect to the quantization axis of the state $|Jm\rangle$,[58] some of them, with relatively small $m'' - m$, being able to contribute to the spin-phonon transition. The coefficients of this decomposition quickly increase with the angle between the main magnetic axes $|-n\rangle$ and $|-n'\rangle$, which is the reason why the spin-phonon relaxation becomes operative via such doublet state.[77] The above analysis also explains why in most single-ion lanthanide complexes the relaxation barrier corresponds to the energy of the first exited doublet state: because of the nonnegligible angle between the main magnetic axes of the ground and first excited doublet states, there will be efficient Orbach and Raman relaxation via the paths $-1 \rightarrow -2 \rightarrow 1$ and $-1 \rightarrow 2 \rightarrow 1$ (Figure 1). The angle between the main magnetic axes of the ground and low-lying excited doublet states can be made small or zero in the presence of strongly dominant axial CF components[89] or symmetry axes, e.g., C_2[93] or near C_5.[94] In such cases, the spin-phonon relaxation via the first or several low-lying excited doublet states can be suppressed. As a matter of fact, relaxation barriers corresponding to the second,[89,93] third,[53] and fourth[94] excited doublet states have been identified in real complexes.

Oblate versus Prolate Ln^{III} Ions. The electronic density in free Ln ions with definite J projection on a given axis is a figure of rotation around this axis, showing state- and ion-specific (nonmonotonic) variation along the polar angle.[95] A qualitative description of the electronic density is achieved for a quadrupolar approximation of its polar angular dependence, in which case the 4f-electron distribution reduces to an ellipsoid of rotation, either prolate (axially elongated) or oblate (equatorially expanded).[37] This simplified description is still able to reproduce the correct stabilization of $|Jm\rangle$ states of Ln ions in environments with preponderant axial and equatorial CF components. For instance, Dy^{3+} has an oblate electron density in the state $\left|\frac{15}{2}, \pm\frac{15}{2}\right\rangle$ and a prolate one in the state $\left|\frac{15}{2}, \pm\frac{1}{2}\right\rangle$.[37] Then the former should be stabilized by an axial CF and the latter by an equatorial CF, which is fully confirmed by the ab initio calculations in Figure 3. In Er^{3+}, the electron distribution is opposite, prolate in the $\left|\frac{15}{2}, \pm\frac{15}{2}\right\rangle$ state and oblate in the $\left|\frac{15}{2}, \pm\frac{1}{2}\right\rangle$ one, with the former being stabilized by equatorial CF and the latter by axial CF, contrary to the situation in Dy^{3+}. The simplest rationalization of this behavior is by invoking the electrostatic interaction of aspherical 4f-electron distribution of Ln ions with the negative electric charges of the surrounding nearest-neighbor ions.[51,96−98] Detailed ab initio analysis does not, however, support this picture, showing instead that the main contribution to the CF splitting of the ground-state atomic J multiplet is of covalent origin.[72] To understand the reason for the strong difference in the stabilization of the ground-state CF multiplet in Dy^{3+} and Er^{3+} complexes, Figure 4 shows the orbital structure of the

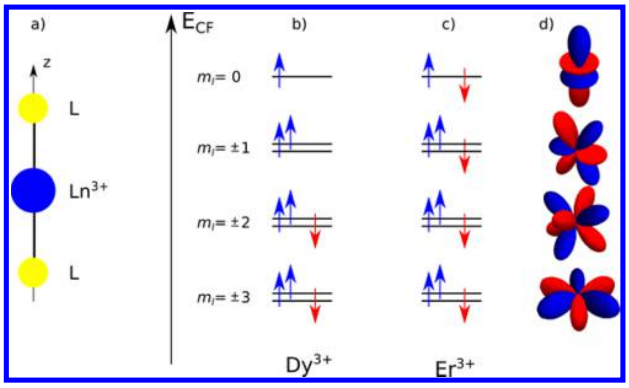

Figure 4. Orbital structure of the $\left|\frac{15}{2}, \frac{15}{2}\right\rangle$ state of Dy^{3+} (b) and Er^{3+} (c) ions in a pure axial CF (a). The levels correspond to seven atomic 4f orbitals split into three orbital doublets, with the projection of the electronic orbital momentum l on the CF axis $m_l = \pm3$, ±2, and ±1 and one orbital singlet with $m_l = 0$. The plots in part d show one real combination of the corresponding $\pm|m_l|$ orbitals. In contrast to them, the density of complex m_l orbitals is invariant with respect to rotations around z.

$\left|\frac{15}{2}, \pm\frac{15}{2}\right\rangle$ state of the two ions in the axial CF. We can see that the two additional spin-down electrons in the electronic configuration of Er^{3+} occupy orbitals with quantum numbers $m_l = -1$ and 0, which are the most destabilized in the axial CF (Figure 4a).[99] This destabilization is caused by a stronger covalent interaction of these orbitals with the ligand ones because of their elongation in the axial direction (Figure 4d)[70] and, to a lesser extent,[72] because of the accompanying stronger electrostatic repulsion from the negatively charged ligands. Thus, destabilization of the orbitals $m_l = -1$ and 0 is the ultimate reason why the CF energy is negative for Dy^{3+} and positive for Er^{3+}.

We will further call the Ln ions oblate or prolate after their electron distribution in the $|J, \pm J\rangle$ states. Figure 3 shows that axial and equatorial CF can provide equally strong splitting of the atomic J multiplets. Therefore, they can both stabilize strongly the $|J, \pm J\rangle$ states of oblate and prolate lanthanides, respectively. Thus, both of these types of Ln ions seem to be good candidates for efficient SMM. In practice, however, there are more chances to achieve large CF splitting and axiality of the doublet states for oblate Ln ions than for prolate ones.

First of all, in the case of a small number of coordinated ligand atoms (n = 1, 2), the Ln−L distances decrease drastically. Indeed, while in the conventional lamthanide complexes (n = 8−12), the Ln−N and Ln−O bond lengths are in the range of 2.1−2.6 Å;[100] in $[DyO]^+$, it is 1.74 Å (Figure 2b). The CF splitting depends strongly on the metal−ligand bond length, first of all, via its covalent contribution, being therefore much larger in diatomic compounds than in conventional lanthanide complexes (Figure 2). On the contrary, the CF strength from the ligands located in the equatorial plane is limited by relatively large Ln−L distances, especially for large n.[54,72,100,101] Thus, in two recently investigated pentagonal-bipyramidal complexes of Dy^{III},[53,57] the bond lengths for the atoms in the equatorial plane are R(Dy−N) = 2.58 and 2.36 Å. As a result, in both complexes, the axial CF component is predominant.[102,103] In equatorially coordinated lanthanide complexes, like three-coordinated $Er[N(SiMe_3)_2]_3$,[104] the CF is purely equatorial. However,

DOI: 10.1021/acs.inorgchem.6b01353
Inorg. Chem. 2016, 55, 10043−10056

only a modest relaxation barrier (122 K) and an overall CF not exceeding 500 cm^{-1} was found for this complex.[104] The sandwich compounds allow one to coordinate more ligand atoms.[35,52,54,105] However, they provide both equatorial and axial CF contributions, which compete with each other, reducing the extent of CF splitting. Thus, in double-decker phthalocyanine complexes,[35,52] the axial component is always predominant, being able to provide a blocking barrier as high as 650 cm^{-1}.[52] Predominant equatorial CF was observed in Cp*ErCOT[105,106] and $Er(COT)_2^-$,[54,55] which, however, have shown modest CF splitting of ca. 300 and 500 cm^{-1}, respectively.

A second argument in favor of oblate ions is that they provide a stronger CF splitting compared to the prolate ones in a similar ligand environment. For instance, $Dy(COT)_2^-$ and $Dy[N(SiMe_3)_2]_3$ display a twice larger CF splitting of the $J = {}^{15}/_2$ multiplet than the isostructural complexes of Er^{3+}.[55,104] This is explained by the relative values of Steven's α_2 and α_4 parameters,[59,60] which are larger (and of opposite sign) for Dy^{3+}. The stronger CF provides a priori higher blocking barriers because of increased separation between the doublet levels and higher axiality of the doublets, as discussed previously.

Finally, it is much easier to provide high rotational symmetry for the axial CF than for the equatorial one. Indeed, a simple connection to one single ligand atom imposes already a perfectly axial CF (of infinite rotational order). At the same time, the engineering of an equatorial CF requires n atoms in the form of a regular polygon in order to have a C_n rotational symmetry. This has been achieved so far for pentagonal-equatorial coordination ($n = 5$).[53] Note that even in this case there will be no doublets of pure Ising form, $|Jm\rangle$, which requires a rotational axis of an order higher than 7. Besides, the high symmetry of such a coordination will be broken when the complex is deposited on a surface.

PRACTICAL SOLUTIONS

From the above analysis, two conclusions concerning the design of efficient single-ion SMMs emerge:

(1) The complexes should provide an efficient single/double atomic axial CF (one/two dominant strongly covalent chemical bonds).

(2) The oblate Ln ions Tb^{3+} and Dy^{3+} (to a lesser extent Ho^{3+}) should be employed.

Following these recommendations, we discuss three approaches of their practical implementation.

Effective Lowering of the Coordination Number. We have seen in the previous chapter that low coordination numbers ($n = 1, 2$) induce large CF splitting and axiality of the CF doublets. However, it is quite rare that lanthanides form compounds with one, two, or even three chemical bonds. At the same time, a situation is often encountered when the lanthanide complexes display magnetization blocking for a low-symmetric ligand environment of the Ln ion. As was pointed out above, besides inducing high axiality in individual low-lying doublets, the CF with strong axial components also tends to align their main magnetic axes to the main CF axis z, along which the axial CF is the strongest,[107] In this way, the main magnetic axes of the low-lying doublets are also forced to align with each other, whereas the resulting small angles between them create the conditions for multilevel blocking barriers (see the fifth section in the previous chapter). This situation arises when the Ln ion interacts much stronger with one (or two trans-coordinated) of the ligand atoms. In this case, the main CF axis will practically pass through that atom, while the closeness of the main magnetic axis of the ground and low-lying excited doublet states to the corresponding M−L bond is a measure of the relative strength of this axial CF component. As an example, Table 1 presents the angles between the shortest M−L bonds and the main magnetic axis of the ground doublet state in a series of performant SMMs involving Dy^{III} ions. Analyzing these data, we notice indeed that the main magnetic axis of the ground KD state on a Dy site makes a small angle with the shortest Dy−X chemical bond, where X is the closest bonding atom. This means that *the anisotropy of the Dy ion is dominantly oriented by the closest ligand atom*. This becomes possible because of the very strong dependence of the CF parameters on the M−L bond length,[70] which makes the CF contribution from an atom with a bond length shorter by several tenths of angstroms absolutely dominant over that of other atoms.

Table 1. Correlation of the Direction of the Main Magnetic Axis with the Shortest Chemical Bond at Dy Sites in Selected Polynuclear Complexes

compound	center	shortest Ln−L bond (Å)	average lengths of all other bonds (Å)	angle of the ground-state anisotropy axis with the shortest bond (deg)	ref
Dy_4	Dy1	2.251	2.466	4.2	109
	Dy2	2.241	2.476	14.0	
Dy_4	Dy1	2.197	2.490	18.5	110
	Dy2	2.195	2.424	16.8	
Dy_2	Dy	2.224	2.522	7.1	111
ZnDyZn	Dy	2.195	2.365	4.1	102
Dy_3	Dy1	2.280	2.484	7.0	112
	Dy2	2.210	2.405	19.9	
	Dy3	2.271	2.492	12.8	
Dy_4K_2	Dy1	2.072	2.353	0.5	89
	Dy2	2.071	2.368	0.7	
	Dy3	2.099	2.377	2.7	
	Dy4	2.114	2.371	2.3	
Dy_5	Dy1	2.075	2.331	5.8	89
	Dy2	1.981	2.567	4.1	
	Dy3	2.150	2.453	2.7	
	Dy4	2.076	2.410	4.7	
	Dy5	1.972	2.335	5.2	
Dy_2Co_2	Dy	2.155	2.413	3.4	113
Dy_2	Dy1	2.125	2.429	10.3	114
	Dy2	2.148	2.493	9.4	
Dy_2	Dy	2.188	2.473	4.1	115

Disregarding for the moment all of the atoms in the molecule except for the closest bonding atom, we arrive at a truly axial DyX complex. As we have seen for the example of $[DyO]^+$ (Figure 2), it displays perfect axiality, with the main magnetic axes parallel to the Dy−O bond in the ground and all excited KD states (except for the one with smallest m) arising from the CF-split atomic $J = {}^{15}/_2$ manifold.[77] Accordingly, magnetization blocking of such a DyX unit is ensured by a multilevel blocking barrier, as discussed in the third section of the previous chapter. The strength (rigidity) of this axial magnetic structure is proportional to the strength of the Dy−X bond. The shorter this bond relative to all other chemical bonds of the Dy^{3+} ion, the harder it is to perturb the axial magnetic structure of the low-lying states (i.e., to induce nonaxial effects: nonzero g_x, g_y,

DOI: 10.1021/acs.inorgchem.6b01353
Inorg. Chem. 2016, 55, 10043−10056

or Δ_{int}). In fact, the role of all other ligand atoms in the molecule, which are generally not collinear with the shortest Dy−X bond, is to increase the nonaxial contribution to the ligand field,[108] perturbing the pure axial states defined by the core Dy−X unit. In this respect, the stronger the effect of the closest ligand (X) and the weaker the overall effect of all of the other ligand atoms, the higher the resulting magnetic axiality of the compound.

To exemplify this effect, we have investigated a model complex $[DyF_6]^{3-}$ with exact octahedral symmetry (Figure 3). We explore the effect of elongation and contraction of *one* of the six Dy−F chemical bonds on the magnetic axiality of the ground KD state of the unit (Figure 5).

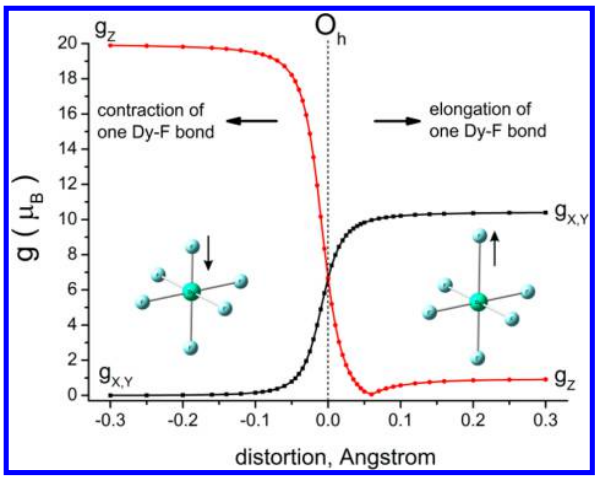

Figure 5. Variation of the main values of the **g** tensor in the ground doublet state of the octahedral $[DyF_6]^{3-}$ complex with the contraction or elongation of one Dy−F chemical bond. Other Dy−F distances were fixed at 2.301 Å, as obtained from the DFT calculations for the octahedral $[GdF_6]^{3-}$ ion.

As one can see in Figure 5, the **g** tensor of the ground doublet state in the octahedral $[DyF_6]^{3-}$ complex is exactly isotropic, with $g_x = g_y = g_z = 6.656$. Upon contraction of one Dy−F chemical bond, we notice a strong increase of the magnetic axiality of the ground doublet state. We may notice that compression of *one* Dy−F chemical bond by just 0.1 Å from the equilibrium bond length is sufficient to make the **g** tensor of the ground KD state strongly axial ($g_{x,y} = 0.15$ and $g_z = 19.5$). In this case, the effect of the F^- ligand, which approaches the Dy^{3+} site, becomes dominant, suppressing the joint effect of all other ligands. As a result, the *ligand field around the* Dy^{3+} *becomes predominantly axial*, corresponding to an effective coordination number of *1*. On the other hand, elongation of one of the Dy−F chemical bonds leads to magnetic anisotropy of the easy-plane type ($g_{x,y} > g_z$) in the ground state. This is because the dominant CF contribution now comes from the closer four equatorial F^- ligands, while the axial CF contribution from a single remaining F^- cannot compensate for their effect. Effectively, the CF felt by the Dy^{III} ion is equivalent to that of a square pyramid.

There are two conditions for a single atom to form a strong chemical bond with a Ln ion. First, it should belong to a monodentate ligand in order to be able to move freely toward the lanthanide. Second, it should make a single bond within its own ligand in order to maximize chemical bonding with the lanthanide. An example is the Dy−O(*tert*-butyl) bond at each Dy site of $[Dy_4K_2O(O^tBu)_{12}]$,[89] and Dy−O(isopropyl) bond at each Dy site in $[Dy_5O(O^iPr)_{13}]$.[116] Figure 6 shows the

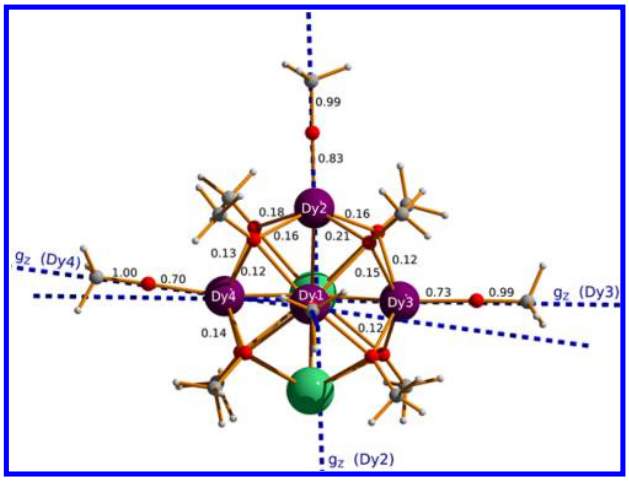

Figure 6. Structure of the Dy_4K_2 complex.[89] Numbers represent the calculated Mayer bond order for the corresponding chemical bond. Notice the much larger bond order for the Dy−O chemical bond with the outer monodentate ligand compared to all other chemical bonds of the corresponding Dy site. Dashed lines show the main magnetic axes in the ground states on individual Dy sites.

calculated Mayer bond orders for the nearest O atoms connecting with one of the Dy ions in the former complex. We can see that the order of the Dy−O bond for the monodentate ligand Dy−O(*tert*-butyl) is 0.73−0.83, which is significantly larger than the bond order to other O atoms from the closest environment, 0.12−0.21. This is due to the reasons given above, (i) the single bond with the nearest C atom (the corresponding bond order is 0.99) and (ii) the freedom to move closer to the Dy ion. As a result, the Dy−O distance for that ligand is only 2.1 Å, i.e., much shorter than that for other nearest-neighbor O atoms (2.3−2.4 Å). In addition, the negative charge at the O atom from the O(*tert*-butyl) ligand is larger than on the other nearest-neighbor atoms (see Figure 6), which further contributes to enhancement of the axial CF.

To conclude, efficient SMMs on the basis of lanthanide complexes with conventional coordination numbers can be obtained via the design of the ligand environment, which provides *one* very short chemical bond with ions Dy^{3+}, Tb^{3+}, and Ho^{3+} or *two* chemical bonds, making an angle of 180° or close to that. At the same time, the effect of all other ligands must be reduced as much as possible.

Two-Coordinated Linear Compounds. As a limiting case of the latter possibility, linear, two-coordinated metal complexes possess intrinsically an axial ligand field. Linear transition-metal complexes are well-known and were obtained with various kinds of ligands. A few of these compounds have shown a strong magnetic blocking phenomenon, a remarkable effect for mononuclear transition ions.[47,63,117] However, stable linear compounds of trivalent Ln ions are not easily obtained, despite significant efforts directed in this area. To date, the only near-linear lanthanide compound is the bivalent Sm^{2+} complex.[91] Predictions of the magnetic anisotropy and blocking capability of several model linear trivalent compounds have been made.[92,118] We further analyze two effects related to a departure from linear bicoordination: the effect of equatorially

DOI: 10.1021/acs.inorgchem.6b01353
Inorg. Chem. 2016, 55, 10043−10056

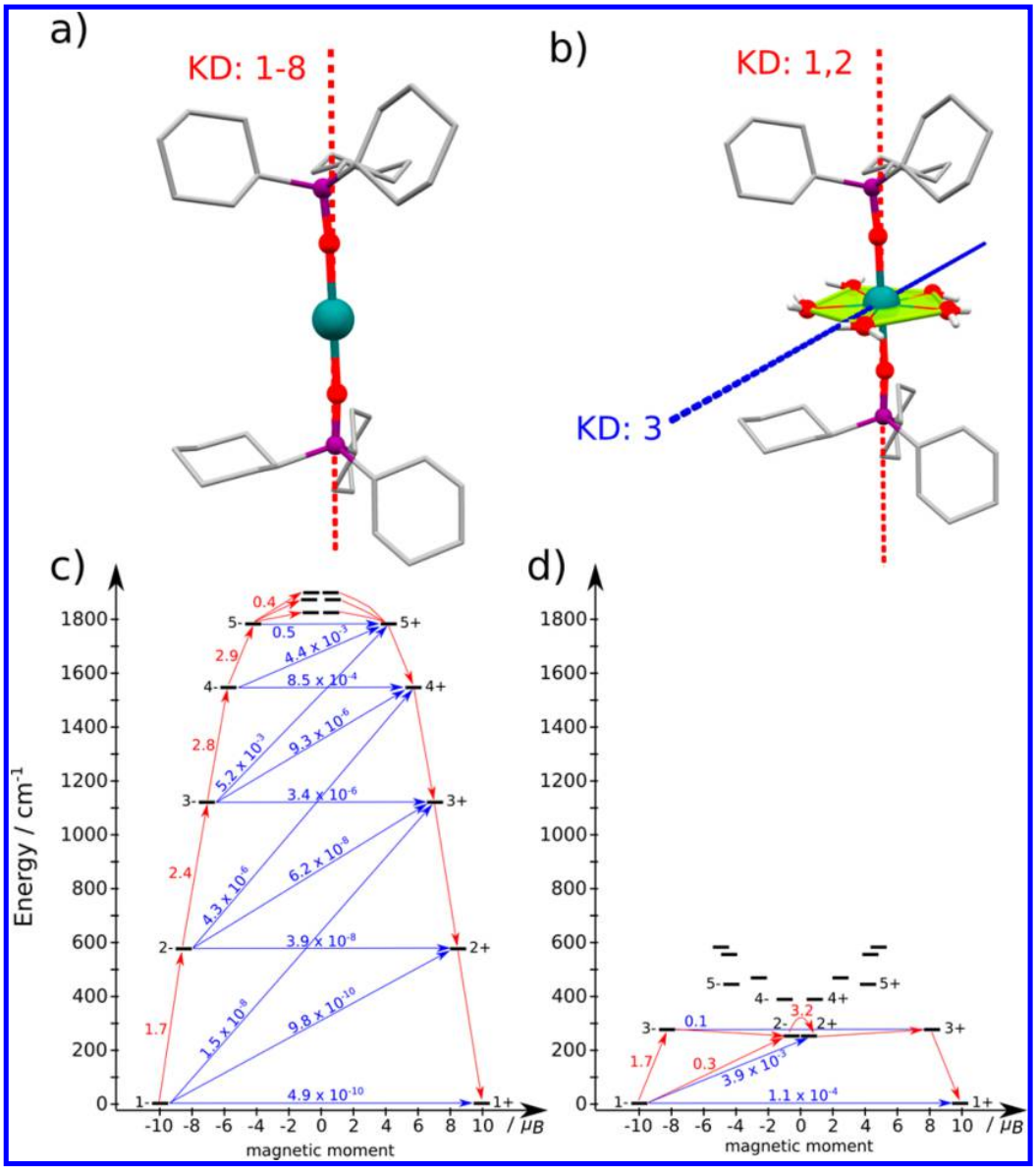

Figure 7. Molecular structure of a mononuclear Dy-D_{5h} compound[57] with the equatorial water molecules removed (a) and in its initial form (b). The dashed lines show the direction of the main magnetic axis of the corresponding KD. Parts c and d show the spectrum of CF doublets and the blocking barrier of reversal of magnetization (red arrows) for the corresponding structures.

bounded ligand/solvent molecules and the effect of the bending of the R−Ln−R core.

Role of the Equatorially Coordinated Solvent Molecules. As an example, we consider the recently reported mononuclear dysprosium compound with near-D_{5h} site symmetry (Figure 7a).[57] In this system, the two axial ligands closely approach the central ion, much more than the five equatorially placed water ligands. Nevertheless, the apparently innocent neutral water ligands hold a crucial destructive effect, drastically reducing the overall blocking barrier and the SMM performance of the complex. Parts c and d of Figure 7 show a comparison between the ab initio calculated blocking barriers of the original molecule in its X-ray geometry and the model molecule, where the five water molecules were removed from the calculation (all other structural details were kept intact). From this comparison, one notices that the overall blocking barrier is reduced several times by the presence of neutral water ligands.

A closer look at the equatorial ligand plane shows that the water molecules are situated quite far from the central metal ion, so that the lone-pair orbitals directed toward the latter will rather contribute to the equatorial component of the CF despite the fact that the two orbital lobes will be arranged in the vertical plane ($\|z$). Removal of the water molecules cancels this equatorial CF contribution, resulting in a larger overall CF splitting, as shown in Figure 7 (compare also Figure 3 for pentagonal-bipyramidal versus two-coordinated linear geometry).

Role of the R−Ln−R Bending Angle. We investigate further the effect of the R−Ln−R bending angle on the resulting blocking barrier of two-coordinated compounds. For this purpose, we chose the structure of a two-coordinated

DOI: 10.1021/acs.inorgchem.6b01353
Inorg. Chem. 2016, 55, 10043−10056

transition-metal compound with a $cAAc^0$ carbene ligand (Figure 8a) with the general formula $[TM(cAAc)_2]^0$, where

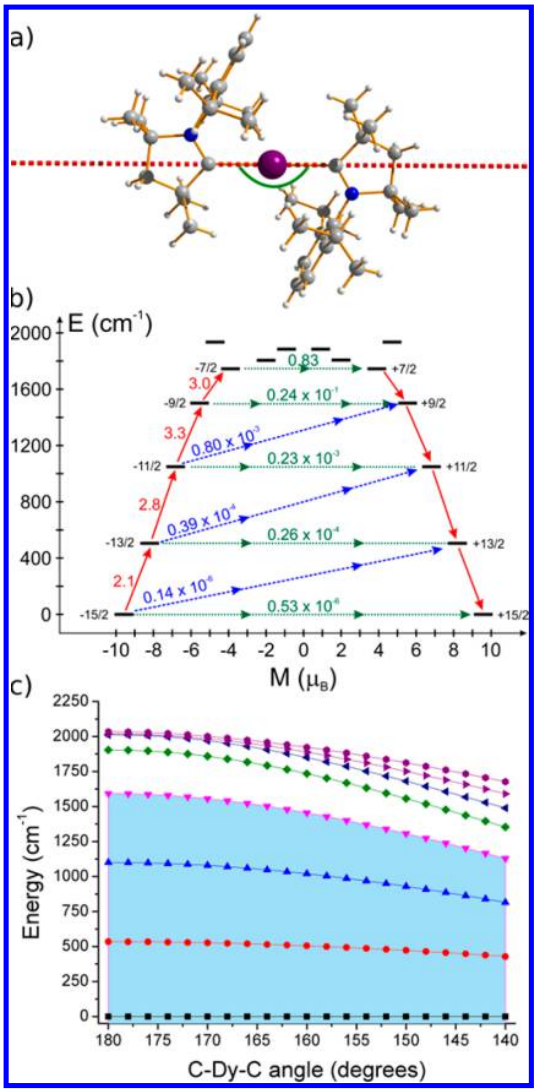

Figure 8. (a) Structure of the model $[Dy(cAAc)_2]^+$ compound. The green arc shows the distortion angle considered here. (b) Magnetization blocking barrier of the undistorted (linear) compound. The black lines represent components of the ground-state $J = {}^{15}/_2$ multiplet, while the arrows connecting them represent the relaxation paths. The number at each path is the average transition dipole moment (eq 5). The red arrows outline the relaxation barrier for the reversal of magnetization. (c) Evolution of the energy spectrum of the ground-state $J = {}^{15}/_2$ multiplet upon bending of the C−Dy−C angle. The highlighted region defines the blocking barrier.

TM = Fe, Mn, and Ni, investigated recently.[119−121] These compounds possess perfect inversion symmetry, with the angle C−TM−C exactly 180°. Here we present the electronic structure, and magnetic axiality of the isostructural $[Dy(cAAc)_2]^+$ compound, assuming that substitution of the transition metal by a Ln^{III} ion is, in principle, possible. The Dy−C bond length was optimized by density functional theory (DFT) to 2.48 Å. Subsequent CASSCF/RASSI/SINGLE_ANISO calculations revealed a high blocking barrier of the resulting model compound in its equilibrium geometry (Figure 8b). Next, similar calculations were performed on structures where the C−Dy−C angle was modified. The resulting low-lying energy spectrum of the ground-state $J = {}^{15}/_2$ multiplet of Dy^{3+} is shown in Figure 8c. The highlighted region in that plot defines the blocking barrier of the deformed structure. We notice that even upon large bending the magnetic axiality of the resulting two-coordinated structure remains quite high, involving at least three excited KD states.

Diatomic Units Deposited on/inside Various Hosts. *a. $[LnX]^{-/0/+}$ Units on Surfaces.* In recent years, several studies appeared in which individual metal atoms were deposited on surfaces, and their properties were investigated. In particular, it was found that the deposited Co atoms on the platinum surface[122] hold large magnetic anisotropy, while their anisotropy is strongest when deposited on the MgO surface.[13] On the other hand, the deposited Ho atoms on the MgO surface also displayed slow magnetic relaxation and magnetic hysteresis.[123] In this section, we show that the deposition of small magnetic units like $[DyX]^{3-n}$, $[TbX]^{3-n}$, or $[HoX]^{3-n}$, where n is the charge of the ligand X = O^{2-}, S^{2-}, Cl^-, F^-, etc., is an even more promising route for the design of efficient SMMs on surfaces. Figure 9 shows the dependence of the blocking

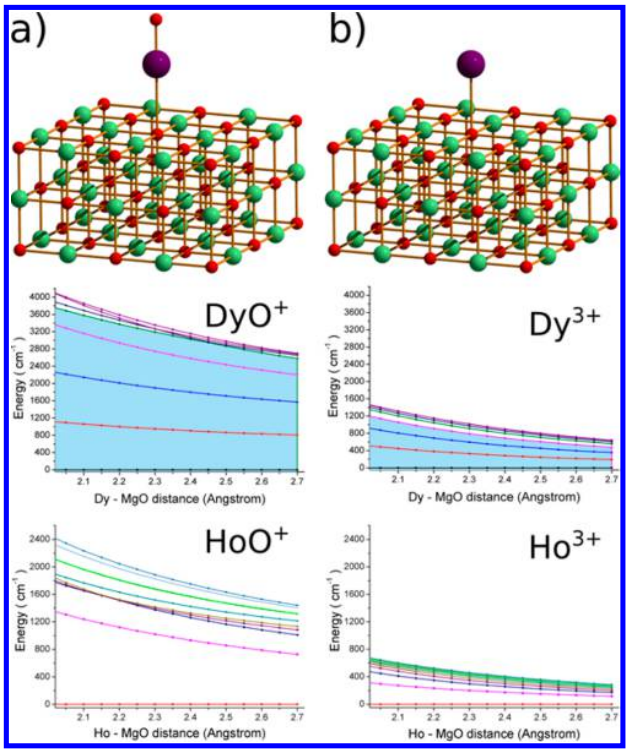

Figure 9. Comparison of the blocking barrier of $[LnO]^+$ (a) with a blocking barrier of Ln^{3+}, where Ln = Dy and Ho, (b) deposited on the MgO surface. For these illustrative calculations, it was assumed that $[LnO]^+$ is oriented perpendicularly to the plane of the surface. Lines in the plots represent the energies of the low-lying $J = {}^{15}/_2$ (Dy) and $J = 8$ (Ho) CF multiplet states.

barrier of the $[LnO]^+$ units on the distance to the MgO surface. For comparison, we performed similar calculations for the deposition of single ions of Ln^{3+}. These calculations show that the blocking barrier of the deposited $[LnO]^+$ is several times larger than that of the deposited Ln^{3+} ion alone. It is important to mention that $[LnO]^{-/0/+}$ are real existing units, with strong

DOI: 10.1021/acs.inorgchem.6b01353
Inorg. Chem. 2016, 55, 10043−10056

chemical bonds between the two atoms, as evidenced by very short equilibrium Ln−O distance obtained in calculations (Figure 2a) and derived from experiments (<1.8 Å). Such units were produced in the gas phase a long time ago and investigated by spectroscopic means.[124−126] We believe that deposition of these units into weakly bound hosts or nonconducting surfaces will not pose problems. In our opinion, the possible change in the oxidation state of the LnO unit, which might happen during such deposition, is unlikely to significantly affect the strong polarization of the orbital momentum on the Ln ion by the neighboring O atom. Further theoretical research in this direction is underway.

b. $[LnX]^{-/0/+}$ Units inside Cages. Another possible way to stabilize diatomic Ln units is to insert them into cages, e.g., fullerenes. In fact, there are a large number of studies where various molecular units and ions are inserted into fullerenes of different sizes.[127,128] We can mention, e.g., $Ln@C_{82}$,[129] $Ln_nSc_{3-n}N@C_{80}$,[130,131] and $Ln_2@C_{79}N$.[132,133] Some of such systems show large barriers for the reversal of magnetization[134] or are predicted to be good SMMs.[133]

In order to show the effect of the cage on the low-lying energy structure of the magnetic unit inserted into a fullerene, we select the previously investigated $DySc_2@C_{80}$ compound as an example.[134] Table 2 shows the ab initio results for the entire compound and for the case when the C_{80} cage is not included in the calculation. In this system, the central N atom produces the dominant ligand-field effect on the Dy site. At the same time, it seems that the role of the cage is rather secondary, i.e., unable to perturb strongly the anisotropy of the already axial magnetic states of the ground and excited KD states. One can observe that the cage increases the total energy splitting of the ground-state $J = {}^{15}/_{2}$ multiplet of Dy^{3+}. We also notice a slight increase of $g_{x,y}$ of the ground and first excited KD states, pointing at a faster QTM relaxation in $DySc_2N@C_{80}$ compared to the free $[DySc_2N]^{6-}$ unit.

Table 2. CF Spectrum and Magnetic Anisotropy of Individual Doublets in $DySc_2N@C_{80}$ and $[DySc_2N]^{6+}$ Entities

$DySc_2N@C_{80}$		$[DySc_2N]^{6+}$	
E (cm^{-1})	g tensor	E (cm^{-1})	g tensor
0	8.3×10^{-5}	0	5.2×10^{-7}
	1.1×10^{-4}		6.4×10^{-7}
	19.86		19.89
415	2.7×10^{-3}	327	1.4×10^{-4}
	2.9×10^{-3}		1.6×10^{-4}
	17.10		17.05
747	2.1×10^{-2}	594	1.7×10^{-2}
	2.9×10^{-3}		2.2×10^{-2}
	14.29		14.21
1002	3.7×10^{-1}	778	0.95
	4.7×10^{-1}		1.60
	11.67		10.34
1158	0.85	864	4.38
	1.60		6.14
	10.34		9.36
1256	7.62	933	3.5×10^{-2}
	5.25		0.21
	1.87		12.65
1334	2.11	1031	1.6×10^{-1}
	5.81		2.8×10^{-1}
	12.50		16.60
1465	1.6×10^{-1}	1135	1.0×10^{-2}
	4.5×10^{-1}		1.7×10^{-2}
	19.14		19.74

Here we show that the insertion of small magnetic units, like $[LnX]^{-/0/+}$, into cages is another promising route toward highly performant SMMs. It is justified to assume that the effect of the cage will remain similar to that in the above example, regardless of the inserted unit: it will lower slightly the magnetic axiality of the ground and low-lying excited states; however, the dominant effect of the X^{n-} ligand on the central metal ion will certainly be preserved. We performed ab initio calculations on a hypothetical $[DyO@C_{60}]^{+}$ complex (Figure 10a). The $[DyO]^{+}$ cation was arranged perpendicular to one of the six-membered rings, with the Dy atom closer to the cage. The distance between the cage and the Dy atom was gradually modified. The resulting energy structure and blocking barrier are shown in Figure 10b. We notice that for any distances between $[DyO]^{+}$ and the cage wall, the magnetization blocking remains significant. As inferred from Figure 3, the corresponding $Dy^{3+}@C_{60}$, with Dy in the central position, would have a large degeneracy in the ground state, with a complete lack of any magnetic anisotropy.

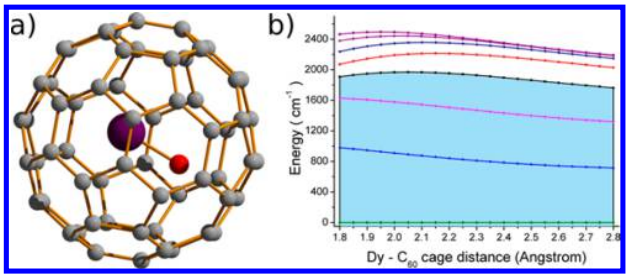

Figure 10. (a) Structure of the hypothetical $DyO@C_{60}$ cation. (b) Blocking barrier of the $DyO@C_{60}$ cation as a function of the distance from the cage.

CONCLUSIONS

Single-ion lanthanide complexes are justifiably considered to be the most promising materials for achieving magnetization blocking at the level of a single molecule. In this paper, we examined the physical requirements for efficient magnetization blocking in such complexes and identified the design principles for achieving very high multilevel magnetization blocking barriers. The key condition is (i) the preponderant covalent binding of the Ln ion to one of the ligand atoms, allowing one to tremendously enhance the axial CF component, and (ii) the use of oblate Ln ions, such as Tb^{3+}, Dy^{3+}, and Ho^{3+}. Another conclusion emerging from the ab initio calculations is that the existence of such a strong CF along a well-defined Ln−ligand direction renders the strict point group symmetry of the lanthanide environment less important. This allows one to obtain strong magnetization blocking on Ln sites in environments that are a priori low-symmetric, such as in polymetallic complexes and under deposition on various surfaces.

We also made an overview of practical schemes for implementation of the above principles. These are (1) the effective lowering of the coordination number via the displacement of a Ln ion toward one of the atoms in the coordination polyhedron, (2) the design of two-coordinated complexes, and (3) the stabilization of diatomic complexes in

DOI: 10.1021/acs.inorgchem.6b01353
Inorg. Chem. 2016, 55, 10043−10056

cages and on surfaces. The last proposal is especially appealing in connection with spintronic applications. This allows the exploration of robust and highly anisotropic [LnX] units, expected to display multilevel blocking barriers of thousands of Kelvin, opening the road to room-temperature magnetization blocking.

AUTHOR INFORMATION

Corresponding Authors

*E-mail: Liviu.Chibotaru@chem.kuleuven.be (L.U.).
*E-mail: Liviu.Ungur@chem.kuleuven.be (L.F.C.).

Notes

The authors declare no competing financial interest.

ACKNOWLEDGMENTS

L.U. is a postdoc of the Fonds Wetenschappelijk Onderzoek-Vlaanderen and also gratefully acknowledges financial support from Methusalem and INPAC grants from the Katholieke Universiteit Leuven. The theoretical chemistry group from Lund University (Prof. P.-Å. Malmqvist and Prof. V. Veryazov) is gratefully acknowledged for hosting L.U. during a research stay.

REFERENCES

(1) Leuenberger, M. N.; Loss, D. *Nature* **2001**, *410*, 789.
(2) Liang, W. J.; Shores, M. P.; Bockrath, M.; Long, J. R.; Park, H. *Nature* **2002**, *417*, 725.
(3) Heersche, H. B.; de Groot, Z.; Folk, J. A.; van der Zant, H. S. J.; Romeike, C.; Wegewijs, M. R.; Zobbi, L.; barreca, D.; Tondello, E.; Cornia, A. *Phys. Rev. Lett.* **2006**, *96*, 206801.
(4) Bogani, L.; Wernsdorfer, W. *Nat. Mater.* **2008**, *7*, 179.
(5) Bertaina, S.; Gambarelli, S.; Mitra, T.; Tsukerblat, B.; Muller, A.; Barbara, B. *Nature* **2008**, *453*, 203.
(6) Ardavan, A.; Blundell, S. J. *J. Mater. Chem.* **2009**, *19*, 1754.
(7) Loth, S.; von Bergmann, K.; Ternes, M.; Otte, A. F.; Lutz, C. P.; Heinrich, A. J. *Nat. Phys.* **2010**, *6*, 340.
(8) Urdampilleta, M.; Klyatskaya, S.; Cleuziou, J.-P.; Ruben, M.; Wernsdorfer, W. *Nat. Mater.* **2011**, *10*, 502.
(9) Candini, A.; Klyatskaya, S.; Ruben, M.; Wernsdorfer, W.; Affronte, M. *Nano Lett.* **2011**, *11*, 2634.
(10) Aromi, G.; Aguilà, D.; Gamez, D.; Luis, F.; Roubeau, O. *Chem. Soc. Rev.* **2012**, *41*, 537.
(11) Vincent, R.; Klyatskaya, S.; Ruben, M.; Wernsdorfer, W.; Balestro, F. *Nature* **2012**, *488*, 357.
(12) Thiele, S.; Balestro, F.; Ballou, R.; Klyatskaya, S.; Ruben, M.; Wernsdorfer, W. *Science* **2014**, *344*, 1135.
(13) Rau, I. G.; Baumann, S.; Rusponi, S.; Donati, F.; Stepanow, S.; Gragnaniello, L.; Dreiser, J.; Piamonteze, C.; Nolting, F.; Gangopadhyay, S.; Albertini, O. R.; Macfarlane, R. M.; Lutz, C. P.; Jones, B. A.; Gambardella, P.; Heinrich, A. J.; Brune, H. *Science* **2014**, *344*, 988.
(14) Ungur, L.; Lin, S. Y.; Tang, J. K.; Chibotaru, L. F. *Chem. Soc. Rev.* **2014**, *43*, 6894.
(15) Das, C.; Vaidya, S.; Gupta, T.; Frost, J. M.; Righi, M.; Brechin, E. K.; Affronte, M.; Rajaraman, G.; Shanmugam, M. *Chem. - Eur. J.* **2015**, *21*, 15639.
(16) Sessoli, R. *ACS Cent. Sci.* **2015**, *1*, 473.
(17) Baumann, S.; Donati, F.; Stepanow, S.; Rusponi, S.; Paul, W.; Gangopadhyay, S.; Rau, I. G.; Pacchioni, G. E.; Gragnaniello, L.; Pivetta, M.; Dreiser, J.; Piamonteze, C.; Lutz, C. P.; Macfarlane, R. M.; Jones, B. A.; Gambardella, P.; Heinrich, A. J.; Brune, H. *Phys. Rev. Lett.* **2015**, *115*, 237202.
(18) Shiddiq, M.; Komijani, D.; Duan, Y.; Gaita-Ariño, A.; Coronado, E.; Hill, S. *Nature* **2016**, *531*, 348.
(19) Gatteschi, D.; Sessoli, R.; Villain, J. *Molecular Nanomagnets*; Oxford University Press: Oxford, U.K., 2006.
(20) Sessoli, R.; Gatteschi, D.; Caneschi, A.; Novak, M. A. *Nature* **1993**, *365*, 141.
(21) Christou, G.; Gatteschi, D.; Hendrickson, D. N.; Sessoli, R. *MRS Bull.* **2000**, *25*, 66.
(22) Mannini, M.; Pineider, F.; Sainctavit, P.; Danieli, C.; Otero, E.; Sciancalepore, C.; Talarico, A. M.; Arrio, M.-A.; Cornia, A.; Gatteschi, D.; Sessoli, R. *Nat. Mater.* **2009**, *8*, 194.
(23) Thomas, L.; Caneschi, A.; Barbara, B. *Phys. Rev. Lett.* **1999**, *83*, 2398.
(24) Friedman, J. R.; Sarachik, M. P.; Tejada, J.; Ziolo, R. *Phys. Rev. Lett.* **1996**, *76*, 3830.
(25) Wernsdorfer, W. *Adv. Chem. Phys.* **2001**, *118*, 99.
(26) Murugesu, M.; Takahashi, S.; Wilson, A.; Abboud, K. A.; Wernsdorfer, W.; Hill, S.; Christou, G. *Inorg. Chem.* **2008**, *47*, 9459.
(27) Rinehart, J. D.; Fang, M.; Evans, W. J.; Long, J. R. *J. Am. Chem. Soc.* **2011**, *133*, 14236.
(28) Gatteschi, D.; Sessoli, R. *Angew. Chem., Int. Ed.* **2003**, *42*, 268.
(29) Garanin, D. A.; Chudnovsky, E. M. *Phys. Rev. B: Condens. Matter Mater. Phys.* **1997**, *56*, 11102.
(30) Villain, J.; Hartman-Boutron, F.; Sessoli, R.; Rettori, A. *Europhys. Lett.* **1994**, *27*, 159.
(31) Novak, M. A.; Folly, W. S. D.; Sinnecker, J. P.; Soriano, S. *J. Magn. Magn. Mater.* **2005**, *294*, 133.
(32) Leuenberger, M. N.; Loss, D. *Phys. Rev. B: Condens. Matter Mater. Phys.* **2000**, *61*, 1286.
(33) Hartmann-Boutron, F.; Politi, P.; Villain, J. *Int. J. Mod. Phys. B* **1996**, *10*, 2577.
(34) Ishikawa, N.; Sugita, M.; Ishikawa, T.; Koshihara, S.; Kaizu, Y. *J. Am. Chem. Soc.* **2003**, *125*, 8694.
(35) Ishikawa, N.; Sugita, M.; Ishikawa, T.; Koshihara, S.; Kaizu, Y. *J. Phys. Chem. B* **2004**, *108*, 11265.
(36) Sessoli, R.; Powell, A. K. *Coord. Chem. Rev.* **2009**, *253*, 2328.
(37) Rinehart, J. D.; Long, J. R. *Chem. Sci.* **2011**, *2*, 2078.
(38) Huang, Y. G.; Jiang, F. L.; Hong, M. C. *Coord. Chem. Rev.* **2009**, *253*, 2814−2834.
(39) Woodruff, D. N.; Winpenny, R. E. P.; Layfield, R. A. *Chem. Rev.* **2013**, *113*, 5110.
(40) Zhang, P.; Guo, Y. N.; Tang, J. K. *Coord. Chem. Rev.* **2013**, *257*, 1728.
(41) Habib, F.; Murugesu, M. *Chem. Soc. Rev.* **2013**, *42*, 3278.
(42) Layfield, R. A., Murugesu, M., Eds. *Lanthanides and Actinides in Molecular Magnetism*; Wiley: Hoboken, NJ, 2015.
(43) Benelli, C.; Gatteschi, D. *Introduction to Molecular Magnetism: From Transition Metals to Lanthanides*; Wiley: Hoboken, NJ, 2015.
(44) Rinehart, J. D.; Long, J. R. *J. Am. Chem. Soc.* **2009**, *131*, 12558.
(45) Freedman, D. E.; Harman, W. H.; Harris, T. D.; Long, G. J.; Chang, C. J.; Long, J. R. *J. Am. Chem. Soc.* **2010**, *132*, 1224.
(46) Magnani, N.; Apostolidis, C.; Morgenstern, A.; Colineau, E.; Griveau, J.-C.; Bolvin, H.; Walter, O.; Caciuffo, R. *Angew. Chem., Int. Ed.* **2011**, *50*, 1696.
(47) Zadrozny, J. M.; Atanasov, M.; Bryan, A. M.; Lin, C. Y.; Rekken, B. D.; Power, P. P.; Neese, F.; Long, J. R. *Chem. Sci.* **2013**, *4*, 125.
(48) Liddle, S. T.; van Slageren, J. *Chem. Soc. Rev.* **2015**, *44*, 6655.
(49) Meihaus, K. R.; Long, J. R. *Dalton Trans.* **2015**, *44*, 2517.
(50) Magnani, N. *Int. J. Quantum Chem.* **2014**, *114*, 755.
(51) Gomez-Coca, S.; Aravena, D.; Morales, R.; Ruiz, E. *Coord. Chem. Rev.* **2015**, *289−290*, 379.
(52) Ganivet, C. R.; Ballesteros, B.; de la Torre, G.; Clemente-Juan, J. M.; Coronado, E.; Torres, T. *Chem. - Eur. J.* **2013**, *19*, 1457.
(53) Liu, J.; Chen, Y.-C.; Liu, J.-L.; Vieru, V.; Ungur, L.; Jia, J.-H.; Chibotaru, L. F.; Lan, Y.; Wernsdorfer, W.; Gao, S.; Chen, X.-M.; Tong, M.-L. *J. Am. Chem. Soc.* **2016**, *138*, 5441.
(54) Meihaus, K. R.; Long, J. R. *J. Am. Chem. Soc.* **2013**, *135*, 17952.
(55) Ungur, L.; Le Roy, J. J.; Korobkov, I.; Murugesu, M.; Chibotaru, L. F. *Angew. Chem., Int. Ed.* **2014**, *53*, 4413.
(56) Donati, F.; Rusponi, S.; Stepanow, S.; Wackerlin, C.; Singha, A.; Persichetti, L.; Baltic, R.; Diller, K.; Patthey, F.; Fernandes, E.; Dreiser, J.; Sljivancanin, Z.; Kummer, K.; Nistor, C.; Gambardella, P.; Brune, H. *Science* **2016**, *352*, 318.

DOI: 10.1021/acs.inorgchem.6b01353
Inorg. Chem. 2016, 55, 10043−10056

(57) Chen, Y.-C.; Liu, J.-L.; Ungur, L.; Liu, J.; Li, Q.-W.; Wang, L.-F.; Ni, Z.-P.; Chibotaru, L. F.; Chen, X.-M.; Tong, M.-L. *J. Am. Chem. Soc.* **2016**, *138*, 2829.
(58) Chibotaru, L. F. In Molecular Nanomagnets and Related Phenomena. *Structure and Bonding*; Gao, S., Ed.; Springer: Berlin, Germany, 2014; Vol. *164*, p 185.
(59) Abragam, A.; Bleaney, B. *Electron Paramagnetic Resonance of Transition Ions*; Oxford University Press: Oxford, U.K., 1970.
(60) Zvezdin, A. K.; Matveev, V. M.; Popov, A. I. *Rare Earth Ions in Magnetically Ordered Crystals*; Nauka, Moskow, 1985 (in Russian).
(61) Langley, S. K.; Wielechowski, D. P.; Vieru, V.; Chilton, N. F.; Moubaraki, B.; Abrahams, B. F.; Chibotaru, L. F.; Murray, K. S. *Angew. Chem., Int. Ed.* **2013**, *52*, 12014.
(62) Prokof'ev, N. V.; Stamp, P. C. E. *J. Low Temp. Phys.* **1996**, *104*, 143.
(63) Atanasov, M.; Zadrozny, J. M.; Long, J. R.; Neese, F. *Chem. Sci.* **2013**, *4*, 139.
(64) Pedersen, K. S.; Ungur, L.; Sigrist, M.; Sundt, A.; Schau-Magnussen, M.; Vieru, V.; Mutka, H.; Rols, S.; Weihe, H.; Waldmann, O.; Chibotaru, L. F.; Bendix, J.; Dreiser, J. *Chem. Sci.* **2014**, *5*, 1650.
(65) Larson, G. H.; Jeffries, C. D. *Phys. Rev.* **1966**, *141*, 461.
(66) Van den Broek, J.; Van der Marel, L. C. *Physica* **1997**, *56*, 11102.
(67) Huang, C.-Y. *Phys. Rev.* **1965**, *139*, A241.
(68) Garanin, D. A.; Chudnovsky, E. M. *Phys. Rev. B* **1963**, *29*, 948.
(69) Gorller-Warland, C.; Binnemans, K. In *Handbook on the Physics and Chemistry of Rare Earths*; Gschneider, K. A., Eyring, L., Eds.; North Holland Publishing Co.: Amsterdam, The Netherlands, 1996; Vol. *23*, p 121.
(70) Figgis, B. N.; Hitchman, M. A. *Ligand Field Theory and its Applications*; Wiley-VCH: New York, 1990.
(71) Rigorous derivation of the CF operator for a given J multiplet by ab initio calculations shows the presence of ranks higher than six in eq 1, due to the effects of metal−ligand covalency and the admixture of excited-state terms, not included in phenomenological CF theory.[72]
(72) Ungur, L.; Chibotaru, L. F. Ab initio crystal field for lanthanides. **2016**, Submitted.
(73) Chibotaru, L. F.; Ungur, L. *J. Chem. Phys.* **2012**, *137*, 064112.
(74) Varshalovich, D. A.; Moskalev, A. N.; Khersonskii, V. K. *Quantum Theory of Angular Momentum*; World Scientific: Singapore, 1988.
(75) Dohm, V.; Fulde, P. *Z. Phys. B: Condens. Matter Quanta* **1975**, *21*, 369.
(76) Luis, F.; Martínez-Pérez, M. J.; Montero, O.; Coronado, E.; Cardona-Serra, S.; Martí-Gastaldo, C.; Clemente-Juan, J. M.; Sesé, J.; Drung, D.; Schurig, T. *Phys. Rev. B: Condens. Matter Mater. Phys.* **2010**, *82*, 060403.
(77) Ungur, L.; Chibotaru, L. F. *Phys. Chem. Chem. Phys.* **2011**, *13*, 20086.
(78) Another relaxation process that directly connects $|-n\rangle$ and $|n\rangle$ is the first-order Raman process.[59] It is also operative for (quasi) degenerate doublet states because its rate is independent of the energy separation between the levels.
(79) Villain, J.; Würger, A.; Fort, A.; Rettori, A. *J. Phys. I* **1997**, *7*, 1583.
(80) Tupitsyn, I. S.; Barbara, B. In *Magnetism: Molecules to Materials III*; Miller, J. S., Drillon, M., Eds.; Wiley-VCH: Weinheim, Germany, 2002; p 109.
(81) Fernández, J. F.; Alonso, J. J. *Phys. Rev. B: Condens. Matter Mater. Phys.* **2000**, *62*, 53.
(82) Wernsdorfer, W.; Caneschi, A.; Sessoli, R.; Gatteschi, D.; Cornia, A.; Villar, V.; Paulsen, C. *Phys. Rev. Lett.* **2000**, *84*, 2965.
(83) Prokof'ev, N. V.; Stamp, P. C. E. *Rep. Prog. Phys.* **2000**, *63*, 669.
(84) Prokof'ev, N. V.; Stamp, P. C. E. *Phys. Rev. Lett.* **1998**, *80*, 5794.
(85) Fernández, J. F.; Alonso, J. J. *Phys. Rev. Lett.* **2003**, *91*, 047202.
(86) Chudnovsky, E. M.; Tejada, J. *Macroscopic Quantum Tunneling of the Magnetic Moment*; Cambridge University Press: Cambridge, U.K., 1998.
(87) Ungur, L.; Thewissen, M.; Costes, J.-P.; Wernsdorfer, W.; Chibotaru, L. F. *Inorg. Chem.* **2013**, *52*, 6328.
(88) A practically equivalent definition of this quantity is $(|\mu_x|^2 + |\mu_y|^2 + |\mu_z|^2)/3$[89] or, equivalently, $(|J_x|^2 + |J_y|^2 + |J_z|^2)/3$.[90,91]
(89) Blagg, R. J.; Ungur, L.; Tuna, F.; Speak, J.; Comar, J.; Collison, D.; Wernsdorfer, W.; McInnes, E. J. L.; Chibotaru, L. F.; Winpenny, R. E. P. *Nat. Chem.* **2013**, *5*, 673.
(90) Lucaccini, E.; Briganti, M.; Perfetti, M.; Vendier, L.; Costes, J.-P.; Totti, F.; Sessoli, R.; Sorace, L. *Chem. - Eur. J.* **2016**, *22*, 5552.
(91) Chilton, N. F.; Goodwin, C. A. P.; Mills, D. P.; Winpenny, R. E. P. *Chem. Commun.* **2015**, *51*, 101.
(92) Ishikawa, N.; Sugita, M.; Wernsdorfer, W. *Angew. Chem., Int. Ed.* **2005**, *44*, 2931.
(93) Guo, Y. N.; Ungur, L.; Granroth, G. E.; Powell, A. K.; Wu, C. J.; Nagler, S. E.; Tang, J. K.; Chibotaru, L. F.; Cui, D. M. *Sci. Rep.* **2014**, *4*, 5471.
(94) Singh, S. K.; Gupta, T.; Shanmugam, M.; Rajaraman, G. *Chem. Commun.* **2014**, *50*, 15513.
(95) Sievers, J. *Z. Phys. B: Condens. Matter Quanta* **1982**, *45*, 289.
(96) Baldovi, J. J.; Borras-Almenar, J.-J.; Clemente-Juan, J. M.; Coronado, E.; Gaita-Arino, A. J. *Dalton Trans.* **2012**, *41*, 13705.
(97) Chilton, N. F.; Collison, D.; McInnes, E. J. L.; Winpenny, R. E. P.; Soncini, A. *Nat. Commun.* **2013**, *4*, 2551.
(98) Sun, W. B.; Yan, P. F.; Jiang, S. D.; Wang, B. W.; Zhang, Y. Q.; Li, H. F.; Chen, P.; Wang, Z. M.; Gao, S. *Chem. Sci.* **2016**, *7*, 684.
(99) Because the CF operator, eq 2, is traceless, the subshell of seven spin-up electrons will not contribute to the CF splitting of $J = {}^{15}/_{2}$ in both Dy^{3+} and Er^{3+} ions. Besides, their common electron density is perfectly spherical. The CF energy and asphericity of the electron density come only from the partly filled subshell of spin-down electrons. Upon superposition of the plots of the respective orbitals (Figure 4d), it is easily seen that the asphericity of the electron density will be of the oblate type for Dy^{3+} and of the prolate type for Er^{3+}.
(100) To be found in the CCDC database: http://www.ccdc.cam.ac.uk.
(101) Le Roy, J. J.; Korobkov, I.; Murugesu, M. *Chem. Commun.* **2014**, *50*, 1602−1604.
(102) Liu, J.-L.; Chen, Y.-C.; Zheng, Y.-Z.; Lin, W.-Q.; Ungur, L.; Wernsdorfer, W.; Chibotaru, L. F.; Tong, M.-L. *Chem. Sci.* **2013**, *4*, 3310−3316.
(103) In the complex with large equatorial Dy−N bond lengths,[53] the resulting equatorial CF is so weak that the uncompensated axial CF from two O atoms on the axial position provides a record blocking barrier of 1025 K.
(104) Zhang, P.; Zhang, L.; Wang, C.; Xue, S.; Lin, S.-Y.; Tang, J. *J. Am. Chem. Soc.* **2014**, *136*, 4484.
(105) Jiang, S.-D.; Wang, B.-W.; Sun, H.-L.; Wang, Z.-M.; Gao, S. *J. Am. Chem. Soc.* **2011**, *133*, 4730.
(106) Boulon, M.-E.; Cucinotta, G.; Liu, S.-S.; Jiang, S.-D.; Ungur, L.; Chibotaru, L. F.; Gao, S.; Sessoli, R. *Chem. - Eur. J.* **2013**, *19*, 13726.
(107) This means that the axial CF parameters B_{20}, B_{40}, and B_{60} are the largest along the chosen axis z, i.e., produce the largest axial CF splitting.
(108) Of course, the noncollinear ligand atoms will also contribute to the axial CF of the Dy−X fragment; however, this is a secondary effect.
(109) Guo, P.-H.; Liu, J.-L.; Zhang, Z.-M.; Ungur, L.; Chibotaru, L. F.; Leng, J.-D.; Guo, F.-S.; Tong, M.-L. *Inorg. Chem.* **2012**, *51*, 1233−1235.
(110) Lin, P. H.; Burchell, T. J.; Ungur, L.; Chibotaru, L. F.; Wernsdorfer, W.; Murugesu, M. *Angew. Chem., Int. Ed.* **2009**, *48*, 9489−9492.
(111) Leng, J. D.; Liu, J. L.; Zheng, Y. Z.; Ungur, L.; Chibotaru, L. F.; Guo, F. S.; Tong, M. L. *Chem. Commun.* **2013**, *49*, 158−160.
(112) Wang, Y. X.; Shi, W.; Li, H.; Song, Y.; Fang, L.; Lan, Y. H.; Powell, A. K.; Wernsdorfer, W.; Ungur, L.; Chibotaru, L. F.; Shen, M. R.; Cheng, P. *Chem. Sci.* **2012**, *3*, 3366−3370.
(113) Mondal, K. C.; Sundt, A.; Lan, Y.; Kostakis, G. E.; Waldmann, O.; Ungur, L.; Chibotaru, L. F.; Anson, C. E.; Powell, A. K. *Angew. Chem., Int. Ed.* **2012**, *51*, 7550−7554.

DOI: 10.1021/acs.inorgchem.6b01353
Inorg. Chem. 2016, 55, 10043−10056

(114) Guo, Y.-N.; Xu, G.-F.; Wernsdorfer, W.; Ungur, L.; Guo, Y.; Tang, J.; Zhang, H.-J.; Chibotaru, L. F.; Powell, A. K. *J. Am. Chem. Soc.* **2011**, *133*, 11948−11951.
(115) Long, J.; Habib, F.; Lin, P.-H.; Korobkov, I.; Enright, G.; Ungur, L.; Chibotaru, L. F.; Wernsdorfer, W.; Murugesu, M. *J. Am. Chem. Soc.* **2011**, *133*, 5319−5328.
(116) Blagg, R. J.; Muryn, C. A.; McInnes, E. J. L.; Tuna, F.; Winpenny, R. E. P. *Angew. Chem., Int. Ed.* **2011**, *50*, 6530.
(117) Zadrozny, J. M.; Xiao, D. J.; Atanasov, M.; Long, G. J.; Grandjean, F.; Neese, F.; Long, J. R. *Nat. Chem.* **2013**, *5*, 577−581.
(118) Chilton, N. F. *Inorg. Chem.* **2015**, *54*, 2097−2099.
(119) Samuel, P. P.; Mondal, K. C.; Amin Sk, N.; Roesky, H. W.; Carl, E.; Neufeld, R.; Stalke, D.; Demeshko, S.; Meyer, F.; Ungur, L.; Chibotaru, L. F.; Christian, J.; Ramachandran, V.; van Tol, J.; Dalal, N. S. *J. Am. Chem. Soc.* **2014**, *136*, 11964−11971.
(120) Samuel, P. P.; Mondal, K. C.; Roesky, H. W.; Hermann, M.; Frenking, G.; Demeshko, S.; Meyer, F.; Stückl, A. C.; Christian, J. H.; Dalal, N. S.; Ungur, L.; Chibotaru, L. F.; Pröpper, K.; Meents, A.; Dittrich, B. *Angew. Chem., Int. Ed.* **2013**, *52*, 11817−11821.
(121) Mondal, K. C.; Samuel, P. P.; Li, Y.; Roesky, H. W.; Roy, S.; Ackermann, L.; Sidhu, N. S.; Sheldrick, G. M.; Carl, E.; Demeshko, S.; De, S.; Parameswaran, P.; Ungur, L.; Chibotaru, L. F.; Andrada, D. M. *Eur. J. Inorg. Chem.* **2014**, *5*, 818−823.
(122) Gambardella, P.; Rusponi, S.; Veronese, M.; Dhesi, S. S.; Grazioli, C.; Dallmeyer, A.; Cabria, I.; Zeller, R.; Dederichs, P. H.; Kern, K.; Carbone, C.; Brune, H. *Science* **2003**, *300*, 1130−1133.
(123) Donati, F.; Rusponi, S.; Stepanow, S.; Wackerlin, C.; Singha, A.; Persichetti, L.; Baltic, R.; Diller, K.; Patthey, F.; Fernandes, E.; Dreiser, J.; Šljivančanin, Ž.; Kummer, K.; Nistor, C.; Gambardella, P.; Brune, H. *Science* **2016**, *352*, 318−321.
(124) Kulikov, N.; Kaledin, L. A.; Kobyliansky, A. I.; Gurvich, L. V. *Can. J. Phys.* **1984**, *62*, 1855−1870.
(125) Linton, C.; Gaudet, D. M.; Schall, H. *J. Mol. Spectrosc.* **1986**, *115*, 58−73.
(126) Liu, Y. C.; Linton, C.; Schall, H.; Field, R. W. *J. Mol. Spectrosc.* **1984**, *104*, 72−78.
(127) Bethune, D. S.; Johnson, R. D.; Salem, J. R.; Devries, M. S.; Yannoni, C. S. *Nature* **1993**, *366*, 123−128.
(128) Shinohara, H. *Rep. Prog. Phys.* **2000**, *63*, 843−892.
(129) De Nadai, C.; Mirone, A.; Dhesi, S. S.; Bencok, P.; Brookes, N. B.; Marenne, I.; Rudolf, P.; Tagmatarchis, N.; Shinohara, H.; Dennis, T. J. S. *Phys. Rev. B: Condens. Matter Mater. Phys.* **2004**, *69*, 184421.
(130) Westerstrom, R.; Dreiser, J.; Piamonteze, C.; Muntwiler, M.; Weyeneth, S.; Brune, H.; Rusponi, S.; Nolting, F.; Popov, A.; Yang, S. F.; Dunsch, L.; Greber, T. *J. Am. Chem. Soc.* **2012**, *134*, 9840−9843.
(131) Westerstrom, R.; Dreiser, J.; Piamonteze, C.; Muntwiler, M.; Weyeneth, S.; Kramer, K.; Liu, S. X.; Decurtins, S.; Popov, A.; Yang, S. F.; Dunsch, L.; Greber, T. *Phys. Rev. B: Condens. Matter Mater. Phys.* **2014**, *89*, 060406.
(132) Fu, W. J.; Zhang, J. Y.; Fuhrer, T.; Champion, H.; Furukawa, K.; Kato, K. T.; Mahaney, J. E.; Burke, B. G.; Williams, K. A.; Walker, K.; Dixon, C.; Ge, J. C.; Shu, C. Y.; Harich, K.; Dorn, H. C. *J. Am. Chem. Soc.* **2011**, *133*, 9741−9750.
(133) Singh, M. K.; Yadav, N.; Rajaraman, G. *Chem. Commun.* **2015**, *51*, 17732−17735.
(134) Vieru, V.; Ungur, L.; Chibotaru, L. F. *J. Phys. Chem. Lett.* **2013**, *4*, 3565−3569.

DOI: 10.1021/acs.inorgchem.6b01353
Inorg. Chem. 2016, 55, 10043−10056